Performance of Soil-Based Controlled Low-Strength Material Prepared with Alkali-Activated Slag and Coal Bottom Ash

Teng He[1], Jiaqi Wu[1], Yuguang Wang[1], Shu Liu[1,2,*] and Bo Li[1,*]

[1]*Department of Civil Engineering, University of Nottingham Ningbo China, 199 Taikang East Road, Ningbo 315100, China*

[2]*Nottingham Ningbo China Beacons of Excellence Research and Innovation Institute, University of Nottingham Ningbo China, Ningbo 315100, China*

Abstract: The utilisation of excavated soil with high moisture and high viscosity faces challenges such as complex dehydration processes and difficult material dispersion. Controlled Low-Strength Material (CLSM) provides a feasible pathway for its dehydration-free resource utilisation. To enhance sustainability, alkali-activated materials can replace Portland cement as the binder in CLSM. However, the influences of activator concentration on CLSM performance remain unclear, and the dispersibility of high-viscosity soil needs further improvement. Therefore, this study develops a novel CLSM using high-viscosity excavated soil and alkali-activated slag, with coal bottom ash (CBA) introduced to improve its dispersibility. Through flowability, setting time, and compressive strength tests, the influences of binder content, alkaline dosage, silicate modulus, soil-to-aggregate ratio, and wet-dry cycles on CLSM performance are systematically investigated, followed by hydration heat and thermogravimetric analyses to reveal the underlying mechanisms. The results demonstrate that increasing the binder content promotes hydration and enhances the mechanical properties of CLSM. CBA can effectively improve flowability but has limited effects on hydration and strength enhancement. Increasing the alkaline dosage accelerates early hydration and increases 7-day compressive strength but may retard later-stage strength development. Reducing the silicate modulus is beneficial to early hydration and performance, whereas a high modulus presents higher later-stage compressive strength. Wet-dry cycles exert dual effects on CLSM through promoting hydration and inducing internal crack propagation, ultimately resulting in strength degradation under wet-dry cycles. This paper provides a theoretical basis and technical reference for the efficient and low-carbon resource utilisation of high-viscosity excavated soil as filling material.

Keywords: CLSM, Excavated soil, Coal bottom ash, Alkaline dosage, Silicate modulus, Wet-dry cycles.

1. INTRODUCTION

With the acceleration of urbanisation, construction activities have become increasingly frequent, leading to an explosive growth in the output of construction waste soil. It was reported that the annual output of the waste soil from construction has exceeded 2.5 billion tons in China [1]. If this waste soil is only disposed of through traditional landfill methods, it occupies a large amount of valuable land resources, posing a severe challenge to land resource conservation in densely populated urban areas [2]. Meanwhile, the high transportation and landfill costs associated with such disposal also bring a heavy economic burden to engineering construction [2]-[3]. Therefore, exploring sustainable and low-cost disposal and resource utilisation paths for waste soil has become a key issue urgently needed in the construction industry.

Among various resource utilisation directions, using construction waste soil as raw material in pavement base filling, block production, and aggregate manufacturing is considered a highly promising technical route [4]-[7]. However, affected by geographical climate and geological conditions, construction waste soil in the southeast coastal areas of China (*e.g.*, Ningbo) generally has the characteristics of high moisture content and high clay particle content [8]. These characteristics bring many difficulties to the treatment of waste soil. On the one hand, high moisture content makes it extremely difficult to dewater the waste soil. Traditional mechanical dewatering, such as plate and frame filter press, has low efficiency and high energy consumption, which makes it difficult to meet the moisture content requirements for subsequent processing [9]. On the other hand, the high viscosity will cause the waste soil to easily agglomerate when mixed with cementitious materials, making it difficult to form a uniform mixture [10], which seriously restricts its practical application.

To solve the above-mentioned problems, Controlled Low-Strength Material (CLSM) has provided a new pathway for the utilisation of construction waste soil due to its advantages of good fluidity, self-compacting property, and controllable strength [11]-[12]. CLSM is usually composed of cementitious materials, aggregates (or waste soil), and water mixed in a certain proportion [13]. In the preparation of traditional CLSM, cement is the most widely used cementitious material, which has mature technology and stable strength development [14]. However, the cement production process consumes a large amount of resources such as limestone and coal, and about 0.8 ton of carbon

*Address correspondence to this author at the Department of Civil Engineering, University of Nottingham Ningbo China, 199 Taikang East Road, Ningbo 315100, China; E-mail: shu.liu@nottingham.edu.cn; bo.li@nottingham.edu.cn

Received on 13-11-2025 Accepted on 24-12-2025 Published on 29-12-2025

E-ISSN: 2819-828X/25

dioxide is emitted for every 1 ton of cement production, making it a typical high-carbon emission industry [15]. Under the background of the "dual carbon" strategy, the high-carbon characteristic of traditional cement-based CLSM is contrary to “low-carbon development”, so it is necessary to utilise an environmentally friendly alternative cementitious system for CLSM.

The alkali-activated cementitious system developed with solid wastes has attracted increasing attention from the academic and engineering circles in recent years due to its dual advantages of “solid waste resource utilisation” and “low-carbon emission reduction” [16]. This system uses industrial solid wastes such as Ground Granulated Blast-furnace Slag (GGBS), copper slag, steel slag, red mud, recycled concrete powder, fly ash as the main raw materials, and activates the active components in the solid wastes by alkali activators (*e.g*., sodium hydroxide, water glass), making them undergo hydration reactions to form hydration products with cementitious properties [17]-[18]. Compared with ordinary Portland cement (OPC), the alkali-activated cementitious system can not only facilitate the efficient consumption of industrial solid wastes but also reduce carbon emissions by approximately 60%–80% for binders and around 20% for concrete products [19]. The environmental benefits of alkali-activated slag can be further enhanced by using appropriate activators. For instance, alkali-activated slag with $Ca(OH)_2$ activator demonstrates approximately 2.4 times lower CO_2 emissions than conventional OPC concrete. Meanwhile, it shows prominent characteristics in terms of high early-age strength and excellent corrosion resistance [20], showing great potential in replacing traditional Portland cement for the preparation of green CLSM.

Preliminary studies have been undertaken on the application of alkali-activated cementitious systems in CLSM. For example, Lee *et al*. [21] investigated the characteristics of alkali-activated CLSM utilising industrial by-products, including fly ash, slag, and bottom ash and revealed the optimal NaOH content of 1.5-2.5% by weight for future re-excavation. However, in alkali-activated materials, the silicate modulus and alkaline concentration of the activator are key factors affecting the hydration reaction process as well as the morphology and amount of hydration products [22]. For instance, Fang *et al*. [22] indicated that increasing the alkaline dosage and silicate modulus are beneficial to enhancing the compressive strength of alkali-activated slag. In addition, Lang *et al*. [23] emphasised that the impact of the alkaline activator changes significantly with the change of the system moisture content, and the optimal alkali activator parameters in the low-moisture content system may no longer be applicable in the high-moisture content system. It is noted that, unlike traditional alkali-activated cementitious materials featuring low moisture content, CLSM, a typical high-moisture content material, possesses inherently different characteristics. At present, there is no systematic study on the influence of alkali dosage and silicate modulus on the workability and mechanical properties of high-moisture content waste soil-based CLSM, which greatly limits its engineering application.

Furthermore, while CLSM, owing to its relatively high moisture content, can partially alleviate the uneven mixing issue caused by the high moisture and viscosity of the soil, the uniformity of the CLSM mixture is closely tied to its water content [24]. To achieve acceptable mixing uniformity for construction needs, a certain increase in water content (compared to the original soil) is often required. However, higher water content directly impairs the mechanical strength of CLSM. For instance, Khadka *et al*., [25] indicated that even minor adjustments to water content can significantly undermine the mechanical performance of CLSM. To mitigate uneven mixing without excessive water addition, existing studies have proposed that incorporating large aggregates into high-viscosity waste soil is an effective solution [26]. Large aggregates can optimise the mixture gradation, break up soil agglomerates to reduce system viscosity, and enhance both mixing uniformity and fluidity [27]. Therefore, incorporating a suitable solid waste material as fine aggregate has become a possible pathway for resolving the mixing uniformity issue of high-viscosity waste soil-based CLSM. Coal bottom ash (CBA) is an industrial by-product derived from coal combustion processes in thermal power plants. It exhibits a particle size distribution analogous to natural sand, where 90% of the particles retained a size smaller than 4.75 mm [28]. It has been considered as a viable alternative to sand aggregate in concrete. Therefore, the incorporation of a specific dosage of CBA into CLSM may yield positive impacts on both its strength and flowability. However, the feasibility of this approach remains to be further verified through systematic experimentation [28]-[29].

Therefore, this study employs typical high-moisture and high-viscosity construction waste soil from Ningbo as the research object, using GGBS as the precursor and sodium hydroxide (NaOH)-water glass (Na_2SiO_3) as the compound alkaline activator to prepare alkali-activated waste soil-based CLSM. CBA is introduced as large particles to improve its dispersibility and flowability. The influences of alkaline dosage and

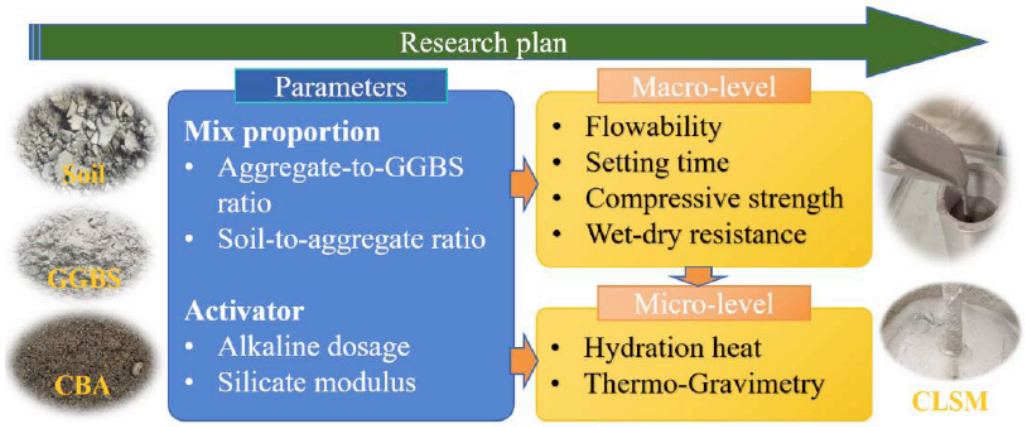

Figure 1: Schematic diagram of research plan.

silicate modulus on the setting time, flowability, and unconfined compressive strength of CLSM are first investigated, followed by a mechanism study based on Thermogravimetric Analysis (TGA) and hydration heat analysis. Finally, the durability of CLSM against wet-to-dry cycles is also examined. This study could provide engineering guidance for the green and efficient utilisation of high-moisture and high-viscosity waste soil.

2. EXPERIMENTAL PROGRAMME

To optimise the mix proportion of CLSM, the overall research plan is shown in Figure **1**.

2.1. Materials and Mix Design

The materials required for CLSM preparation in this study include construction waste soil, CBA, GGBS, alkaline activator, and water. Among them, the construction waste soils are collected from Yuyao, Ningbo, China and are generated from the construction of bored piles for expressways. The CBA was obtained from Ninghai Power Plant, Ningbo, China. Prior to use, the CBA was sieved (2.36 mm in mesh) to remove oversized particles. Figure **2** depicts the particle size distribution of soil and CBA, with an initial moisture content over 60%. The mineral composition and chemical composition of the soil and CBA are given in Figure **3** and Table **1**, respectively. It can be found that Quartz and Mullite are identified as the main components in both materials, while CBA contains a rare mineral Omongwaite.

As the precursor of the alkali-activated binder, GGBS used in Wu *et al*. [30] was adopted in this study. The alkali activator was prepared by mixing sodium hydroxide (NaOH) pellets, sodium silicate (Na_2SiO_3) solution, and water. sodium silicate solution consists of 26.8% SiO_2, 8.3% Na2O and 64.9% H_2O by mass.

The mix design of the CLSM is presented in Table **2**. The mixtures were designed by considering four key parameters: aggregate-to-GGBS ratio, soil-to-aggregate ratio, alkaline dosage, and silicate modulus. The aggregate-to-GGBS ratio is the mass ratio of aggregate to GGBS, where aggregate mass refers to the total mass of soil and CBA. The soil-to-aggregate

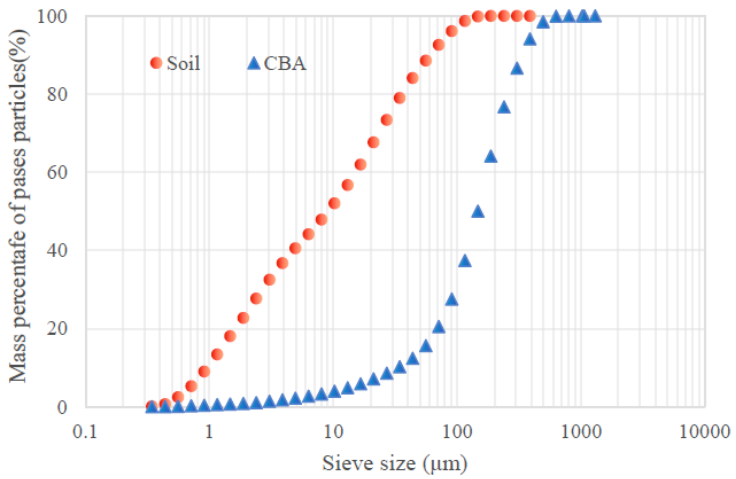

Figure 2: Gradation curves of the excavated soil and CBA.

ratio is the mass ratio of soil to the combination of soil and CBA. The CBA content is controlled at three levels (0, 25%, and 50%) to evaluate its impact on dispersing high-moisture and high-viscosity soil through shearing cohesive fine particles. Throughout all mix designs, the water-to-solid ratio was set to a constant value of 0.55.

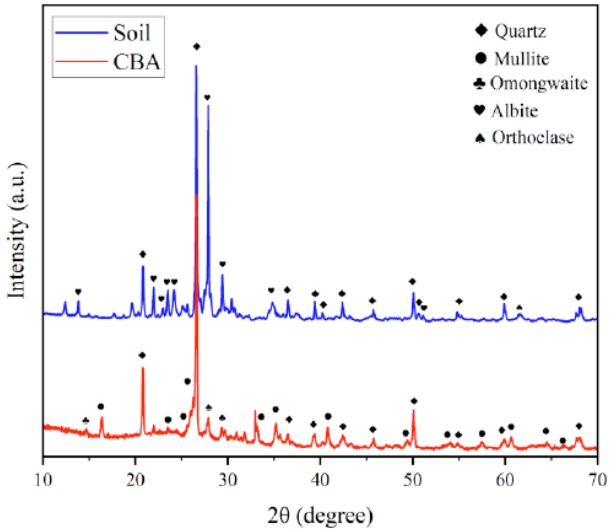

Figure 3: XRD patterns of the excavated soil and CBA

Regarding the naming rule, taking the control group (B15S75 (N8M1)) as an example, "B15" corresponds to an aggregate-to-binder ratio (A/B) of 5.67 (*i.e.*, A = 85%; B = 15% and A/B = 5.67; "B" is the mass ratio of GGBS, which is defined as "binder content" in the following work), "S75" represents a soil-to-aggregate ratio (S/A) of 0.75, "N8" denotes an alkaline dosage of 8.0%, and "M1" indicates a silicate modulus (Ms) of 1.0. Parameters not labelled in a sample name (*e.g.*, B20S75 lacks N and M labels) remain consistent with the control group (*i.e.*, alkaline dosage = 8.0%, Ms = 1).

2.2. Specimen Preparation

Prior to CLSM sample preparation, the alkaline activator was first prepared based on the alkaline dosage and silicate modulus. The preparation method can be referred to [31]. Sodium hydroxide pellets were dissolved in deionised water under gentle stirring to prepare a NaOH solution with the predetermined concentration. The solution was then mixed with sodium silicate solution and additional deionised water at a designed volume ratio. After preparation, the alkaline activator was cooled to room temperature and stored for subsequent use.

Meanwhile, the construction waste soil shall be dried to a constant weight. Subsequently, a predetermined amount of water (*i.e.*, water excluding that contained in the alkali activator solution) shall be added to the dried soil in accordance with the mix design in Table **2**. The mixture shall then be stirred uniformly using a mixer and sealed for preservation to obtain "wet soil", which is set aside for later use.

Once both the wet soil and alkaline activator are prepared, the wet soil is weighed and mixed with half of the alkaline activator. A 5-min low-speed stirring process was applied to ensure uniformity of the mixture. Afterwards, the pre-mixed blend of GGBS and CBA,

Table 1: Chemical Composition of CBA and Soil (%)

Comp.	SiO_2	Al_2O_3	Fe_2O_3	K_2O	CaO	MgO	Na_2O	TiO2	P_2O5	SO_3	Others
Soil	62.06	17.81	6.03	5.15	4.29	1.61	0.89	0.79	0.64	/	0.73
CBA	51.15	25.78	6.12	1.61	8.07	1.08	0.77	0.92	0.96	3.14	0.40

Table 2: Mix Proportions of the CLSM

Mix ID	Aggregate-to-GGBS Ratio	Soil-to-Aggregate Ratio	Alkaline Dosage	Silicate Modulus
Control group B15S75 (N8M1)	5.67	0.75	8.00%	1
B20S75	4.00			
B10S75	9.00			
B15S50	5.67	0.50		
B15S100		1.00		
N6M1		0.75	6.00%	
N10M1			10.00%	
N8M0.75			8.00%	0.75
N8M1.25			8.00%	1.25

along with the remaining alkaline activator, was added to the wet soil mixture. Stirring is continued at a low speed for another 2 mins, after which the mixer speed is increased, and mixing is sustained for an additional 5 mins to complete the CLSM mixture preparation.

2.3. Testing Methods

2.3.1. Flowability

The flow characteristics of CLSM were assessed using the method outlined in ASTM D-6103 [32]. A plastic plate and a cylindrical mould (inner diameter = 100 mm; height = 150 mm) were employed for the test. The mould was first filled with the fresh CLSM, followed by lifting the mould vertically within 2 seconds. The spread dimensions of CLSM across the plate were recorded along two orthogonal directions, and the averaged reading was defined as the flowability of CLSM.

2.3.2. Setting Time

The setting time of CLSM was measured by a Vicat instrument in accordance with GB/T 1346 [33]. After placing the fresh CLSM under the test needle and recording the initial pointer reading, this measurement was then repeated every hour until the reading no longer changes. The time taken to reach such a state is recorded as the setting time.

2.3.3. Unconfined Compressive Strength

For unconfined compressive strength (UCS) tests, freshly prepared CLSM was poured into plastic cylindrical moulds featuring a diameter of 50 mm and a height of 100 mm. The prepared samples were then sealed and cured at 20 °C and 95% relative humidity until the targeted curing age (*e.g.*, 7 or 28 days). UCS tests were conducted following the specifications outlined in ASTM D4832 [34] with a universal testing machine featuring a 50 kN loading capacity, at a constant loading rate (1 mm/min). Three duplicate samples were tested to confirm the reliability of compressive strength test data.

2.3.4. Durability Under Wet-Dry Cycles

Wet-dry cycle tests were conducted with reference to ASTM D559 [35], with appropriate modifications to align with the practical service environment of CLSM. The specific test protocol was defined as follows: one complete wet-dry cycle consisted of two stages: (1) wetting stage: the cured CLSM samples were fully submerged in tap water (20 ± 2 °C) for 5 h to simulate water immersion conditions in engineering scenarios (*e.g.*, subgrade rainfall infiltration); (2) drying stage: after wetting, samples were moved into a constant-temperature/humidity chamber at 20 ± 2 °C and 70% relative humidity for 43 h. The CLSM samples under wetting and drying stages are shown in Figure **4**. The UCS were measured after 4, 8 and 12 wet-dry cycles to evaluate the damage status.

2.3.5. Microstructure Analysis

(1) Hydration heat

The fresh CLSM mixture was used for hydration heat tests. The heat release history during the hydration reaction of CLSM was monitored using a calorimeter (I-Cal 8000 HPC, Calmetrix). The detection process was conducted in a constant-temperature environment of 20 ± 0.01 ºC, with continuous recording of heat release signals over a 28-day period to capture the full hydration process. Afterwards, the hydration heat flow rate, as well as the cumulative heat, was normalised by the solid mass of the CLSM.

(2) TGA

The CLSM specimens were first crushed and sieved, then submerged in isopropanol for more than 24 hours to halt ongoing chemical reactions. Following this, the specimens underwent vacuum drying at 40 ºC for 5 hours. The dried samples were further ground into fine powders, which were then sieved using a 40 μm mesh to achieve particle uniformity [31]. The reaction products of CLSM subjected to 28-day curing and those further subjected to 12 wet-dry cycles were

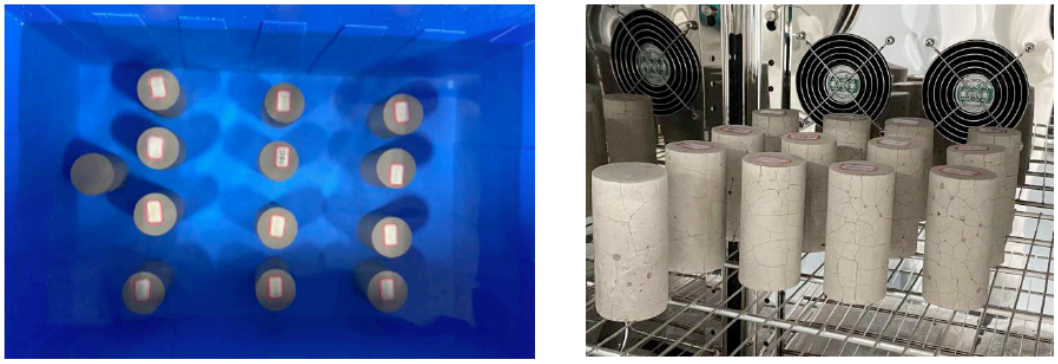

(a) Wetting stage (b) Drying stage

Figure 4: Durability test for CLSM subjected to wet-dry cycles.

determined using a synchronous thermal analyser (EXSTAR 6000 TG/DTA 6300, Seiko). During the test, a nitrogen atmosphere (flow rate = 50 mL/min) was used to avoid oxidative interference. The temperature range was controlled at 30~800 ºC. The heating rate was 10 ºC/min, ensuring consistent thermal conditions for accurate characterisation of reaction products across different samples.

3. RESULTS AND DISCUSSION

3.1. Flowability

Figure **5** summarises the effect of mix design factors on the flowability of the CLSM. The effect of binder content on the flowability of the CLSM is first investigated, with results presented in Figure **5(a)**. It is readily seen that the variation of binder content exerts a slight influence on flowability, demonstrating that higher binder content corresponds to larger flowability. When the binder content increases from 10% to 20%, flowability rises by 10.8%. This can be attributed to the reduced total surface area of solid particles (*e.g.*, GGBS, soil, and CBA), which requires less water to maintain the flowability. Differently, the variation of soil-to-aggregate ratio has a more obvious impact on flowability than any other factors (Figure **5**(**b**)). As the soil-to-aggregate ratio decreases from 50% to 100% (*i.e.*, as CBA content increases from 0% to 50%), the flowability drops drastically from 320 mm to 180 mm. This is likely caused by the coarser particle sizes of CBA, which also require less water to maintain the flowability. For the concentration of the activator, changes in alkaline dosage (Figure **5**(**c**)) or silicate modulus (Figure **5**(**d**)) have marginal impacts on flowability.

3.2. Setting Time

The increase of binder content effectively reduces the setting time, as seen in Figure **6(a)**. Specifically, a rise of the binder content from 10% to 15% decreases the final setting time by 35.1% (from 115.5 to 75.0 hours). This could be directly caused by the enhanced reaction with more binder, which will be further evidenced in the section on reaction heat analyses. However, the magnitude of this reduction becomes negligible as the binder content further increases to 20%. This could be caused by that the available alkali is not enough to fully dissolve and activate all the GGBS particles [36]. The change of soil-to-aggregate ratio also exerts a significant influence on the final setting time (Figure **6**(**b**)). As the soil-to-aggregate ratio increases from 50% to 100% (*i.e.*, as CBA content decreases from 50% to 0%), the setting time decreases significantly from 110 hours to 60 hours. This could be caused by the acceleration effect of the fine powder in CBA on the hydration process [37]. The underlying mechanism will be further discussed below, in combination with the characterisation results. Regarding the alkaline dosage, increasing the alkaline dosage reduces the final settling of the CLSM (Figure

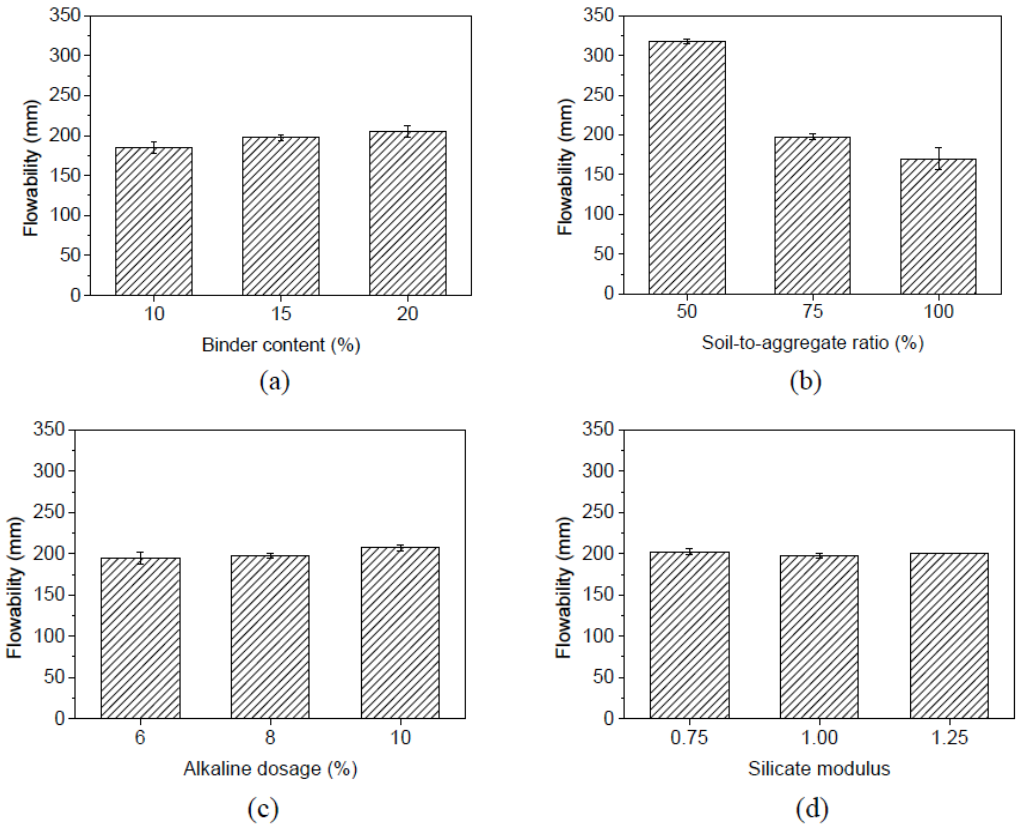

Figure 5: Flowability of the CLSM.

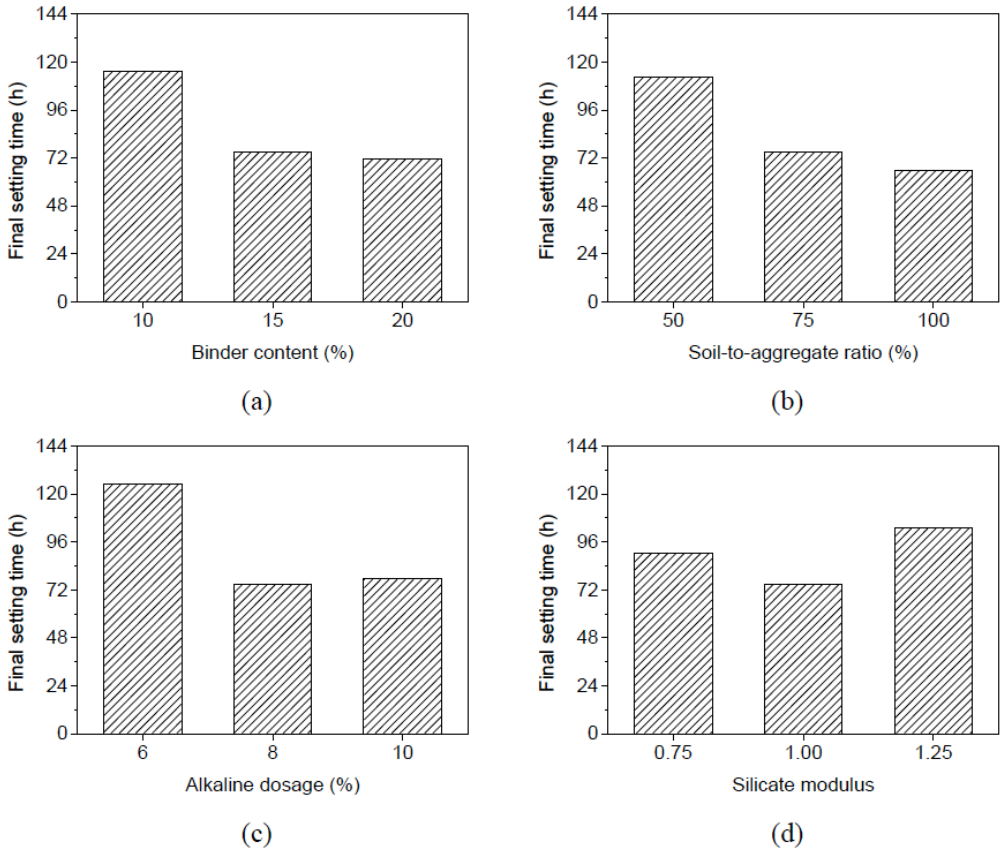

Figure 6: Setting time of the CLSM.

6(**c**)). The final setting time drops from 125 hours to around 75 hours as the alkaline dosage increases from 6% to 8%, which could be attributed to the enhanced reaction process and the formation of more hydration products [38]. However, further elevating the alkaline dosage from 8% to 10% results in a marginal change in the final setting time. The reason could be that the system reaches a state where the available reactive sites are fully utilised, and additional activator does not contribute to further acceleration of the setting process [39]. Moreover, the final setting time first decreases and then increases with the gradual increase of the silicate modulus (Figure **6**(**d**)). A decrease in the silicate modulus from 1 to 0.75 may lead to insufficient reactive silicate species for the rapid formation of binding gels, thereby delaying the setting time [40]-[41].

3.3. Unconfined Compressive Strength

The effect of binder content (*i.e.*, mass ratio of GGBS to solid) on the UCS is given in Figure **7(a)**. It can be observed that with the increase in binder content from 10% to 15%, the 7-day compressive strength is significantly improved from 0.04 MPa to 1.14 MPa. A more significant improvement to 4.05 MPa is observed when the binder content changes from 15% to 20%. Similarly, the 28-day UCS of the CLSM increases from 2.10 MPa to 9.24 MPa as the binder content increases from 10% to 20%. This could be attributed to the promoted alkaline reaction within the CLSM system. The detailed mechanism will be discussed by integrating the hydration reaction and the TGA results. Comparatively, the 28-day compressive strength of the developed CLSM is much higher than that prepared with OPC and pozzolanic materials (< 1.0 MPa) in the literature [11]. Notably, the compressive strength of the CLSM is comparable to that of CBA stabilised by alkali-activated slag [21]. It indicates the excavated soil can be utilised for producing CLSM in conjunction with CBA. Moreover, increasing the soil-to-aggregate ratio could slightly reduce the compressive strength, as seen in Figure **7(b)**. In contrast to soil particles, the fine fraction of CBA is capable of undergoing weak pozzolanic reactions [37], which in turn exerts a moderate positive effect on the strength development of CLSM.

The effect of alkaline dosage on the UCS of the CLSM is illustrated in Figure **7(c)**. It can be seen that an increase in alkaline dosage exerts an obvious enhancing effect on the 7-day UCS of CLSM, which is improved by 356% owing to the improved dissolution efficiency of GGBS and the accelerated formation of binding gels [42]-[43]. Compared to its effect on 7-day compressive strength, its impact on 28-day strength is less significant. However, a notable improvement is still observed when the alkaline dosage increases from 6% or 8% to 10%, ultimately reaching a value of 7.90 MPa. Similarly, (Figure **7**(**d**)) shows that the effect of silicate modulus on compressive strength is more pronounced

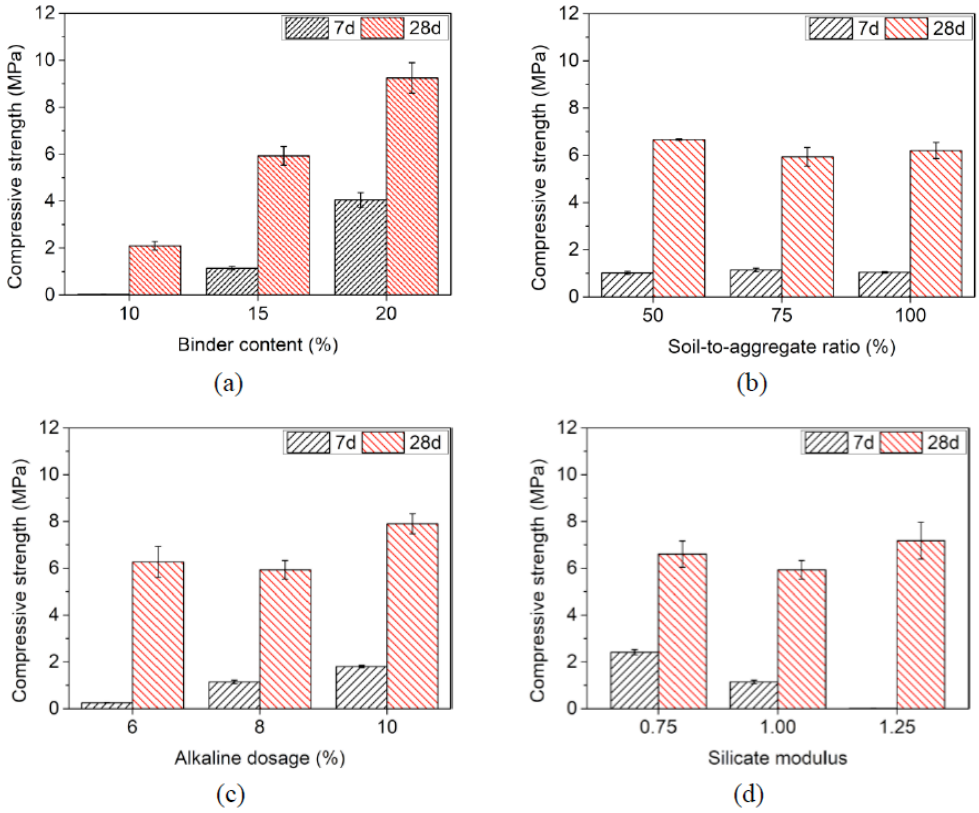

Figure 7: UCS of the CLSM.

for 7-day compressive strength. A higher silicate modulus reduces the compressive strength, causing CLSM to have almost no strength after 7 days of curing. This could be primarily because an excess of silicate ions reduces the pH of the alkaline solution, inhibiting the dissolution of GGBS and therefore the reaction rate of binder at early age [44]-[45]. In addition, although an increased silicate modulus results in low 7-day UCS, it significantly improves 28-day compressive strength, yielding the highest value among all tested groups. The underlying reason will be further analysed in subsequent sections, in combination with microstructure characterisation results.

3.4. Stability of CLSM under Wet-Dry Cycles

The impact of wet-dry cycles on UCS of the CLSM with various binder contents is discussed in this section. The wet-dry cycles reflect the actual field conditions, such as backfill or subgrade exposed to underground water circulation. A lower reduction in UCS indicates better resistance to these wet-dry cycles. Figure **8(a)** indicates that as the binder content increases, the variation in UCS after exposure to wet-dry cycles becomes more pronounced. After 4 wet-dry cycles, the UCS values of both mixes B10S75 and B15S17 change slightly. In contrast, a significant increase in UCS is observed for mix B20S75. This could be caused by that the wetting exposure stage promoted subsequent hydration processes, leading to more hydration products [46]. When the number of wet-dry cycles increases to 8 or 12, slight decreases in UCS were observed for both mixes B10S75 and B15S17. However, mix B20S75 exhibits a significant strength drop. This behaviour could be attributed to the high strength of B20S75, which is associated with increased shrinkage caused by its denser microstructure. Consistent with findings from prior studies on alkali-activated pastes [47]-[48], this densification-induced shrinkage makes mix B20S75 more vulnerable to wet-dry cycles.

The influence of the soil-to-aggregate ratio on UCS of the CLSM subjected to wet-dry cycles is summarised in Figure **8(b)**. A slight improvement on UCS is observed for the mixes B15S50 and B15S100 after 4 wet-dry cycles. In contrast, a slight decrease is observed for mix B15S75 under the same conditions. With an increasing number of wet-dry cycles, no significant changes in UCS are detected for mixes B15S50 and B15S75 after 8 wet-dry cycles. However, a significant decrease is observed for mix B15S100. These results indicate that the incorporation of CBA into the CLSM system enhances the material resistance against wet-dry cycles. On one hand, this could be attributed to the finer particle size and stronger hydrophilicity of soil compared with CBA, which causes more significant shrinkage under wet-dry cycles [49], which leads to extensive crack propagation and thus greater strength reduction in soil. On the other hand, previous studies have identified CBA as an internal curing material in cementitious materials, as its

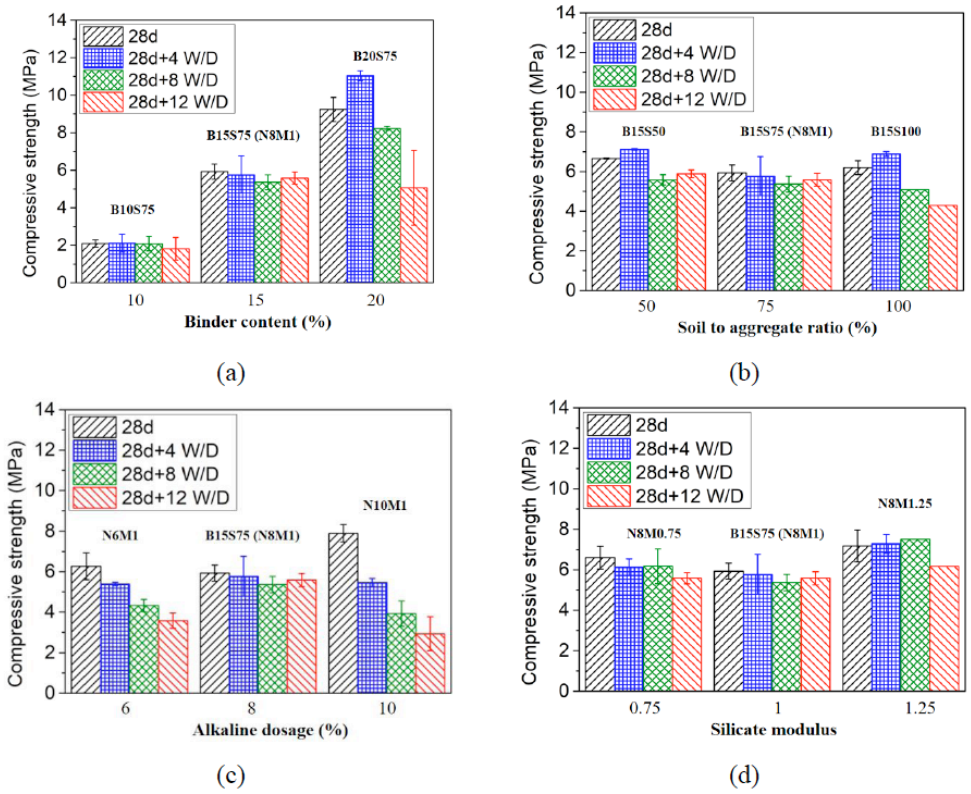

Figure 8: Unconfined compressive strength of the CLSM subjected to wet-dry cycles.

porous structure is leveraged to effectively mitigate shrinkage [50]. In the CLSM developed herein, the enhanced resistance to wet-dry cycles could benefit from the improved shrinkage resistance.

Regarding the effect of alkaline dosage, there exists an optimal dosage (8%) at which the impact of wet-dry cycles is minimised (Figure **8(c)**). The reason may be that a lower activator concentration leads to incomplete dissolution of aluminosilicate precursors and fewer binding gels [42], while a high alkaline dosage accelerates the reaction but also promotes cracking, making the material more sensitive to wet-dry cycles. Moreover, as shown in Figure **8(d)**, the effect of silicate modulus on wet-dry resistance after 12 cycles is not very obvious. Nevertheless, a higher silicate modulus can improve strength under a lower number of wet-dry cycles (*e.g.*, 4 or 8 cycles).

3.5. Hydration Heat Characteristics

The hydration heat results of the CLSM are given in Figure **9**. The impacts of binder content on the heat release rate and cumulative hydration heat are illustrated in Figure **9(a)** and **9(b)**, respectively. Mix B20S75 exhibits the highest and earliest peak heat release rate compared to the other two CLSM with fewer binders. This behaviour could arise from the abundant reactive aluminosilicate components in high-dosage GGBS, which accelerate the dissolution and thus promote rapid early-stage reaction [51]. In contrast, mixes B10S75 and B15S75 display muted peak heat release rates and delayed reaction onsets, as the limited reactive components restrict the reaction process. Correspondingly, the cumulative hydration heat curve (Figure **9(b)**) reveals that B20S75 accumulates more hydration heat than mixes B15S75 and B10S75 over 28 days. This reflects a higher extent of reaction and more amorphous gels (*e.g.*, C-(A)-S-H), which agrees with the TGA results given in the subsequent section. These hydration heat results are in line with the mechanical and setting properties of the CLSM. Specifically, mix B10S75 demonstrates the lowest 7-day and 28-day UCSs, alongside the longest final setting time, across all three formulations. In contrast, mix B20S75 achieves superior 7-day and 28-day compressive strengths and exhibits the shortest final setting time.

The effects of replacing soil with CBA on the reaction heat results of the CLSM are given in Figure **9(c)** and **9(d)**. As seen in Figure **9(c)**, mix B15S50 exhibits a higher and earlier heat release rate peak compared to mix B15S100. This indicates that the use of CBA in CLSM can accelerate the hydration reaction [52]. The reason could be that the reactive aluminosilicate components in CBA can dissolute in an alkaline environment, releasing aluminium (Al) and silicon (Si) ions for the formation of more hydration products in the early stage [53]. In contrast, mix B15S100 shows the weakest and most delayed peak, as inert soil cannot contribute to the reaction. The cumulative hydration heat curve (Figure **9(d)**)

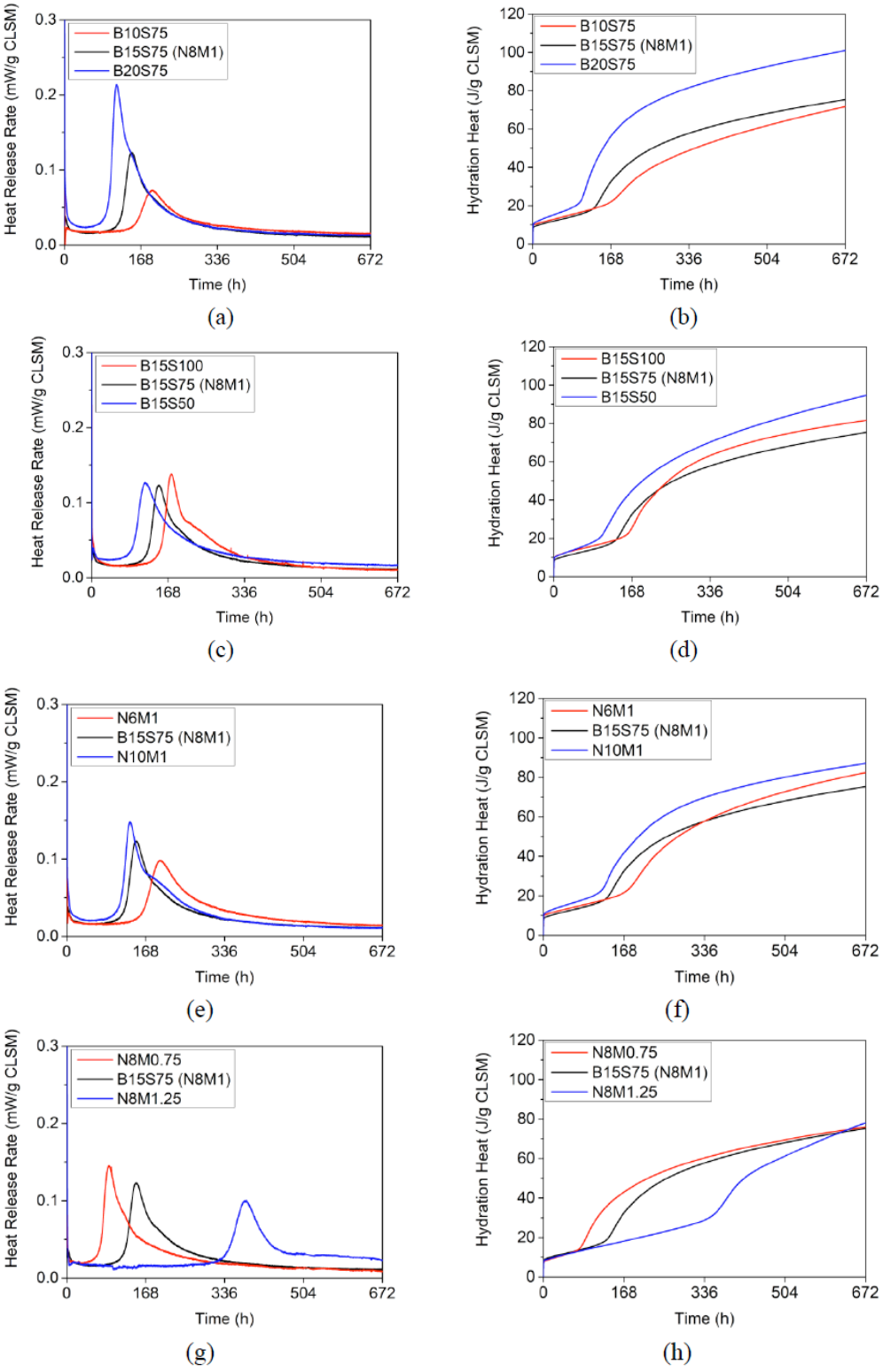

Figure 9: Hydration heat release of the CLSM.

demonstrates that mix B15S50 accumulates significantly more hydration heat than mix B15S100 over 28 days. This indicates that CBA incorporation promotes the formation of additional hydration products, consistent with the TGA results, though this is not the sole factor governing the strength development of CLSM. However, comparing with Figure **9(a)** and **9(c)**, even though CBA can increase the system reaction, its effect is still very limited. At the final stage, the cumulative hydration heat of mix B15S50 is slightly higher than that of mix B15S100, which aligns with the UCS results, where the 28-day UCS of mix B15S50 is slightly higher than that of mix B15S100.

The effects of alkaline dosage on the hydration heat release of CLSM are shown in Figure **9(e)** and **9(f)**. As the alkaline dosage increases from 6% (N6M1) to 10% (N10M1), the early-stage heat release rate peak

becomes higher and appears earlier. For example, mix N10M1 exhibits the most intense peak, while mix N6M1 shows a weaker and delayed peak. This indicates that higher alkaline dosage accelerates the early reaction, as the alkalis promote the dissolution of reactive aluminosilicate components from GGBS via increased solution pH [44]-[45]. Based on the cumulative hydration heat in Figure **9(f)**, mix N10M1 accumulates the most heat over 28 days. However, even though mix N8M1 exhibits higher heat release efficiency and cumulative heat than mix N6M1 in the early stage, after 336 hours, the cumulative heat of mix N6M1 surpasses that of mix N8M1. These results align with the compressive strength data: that mix N10M1 yields the highest 7-day and 28-day UCS, while mix N8M1 shows a higher 7-day compressive strength than mix N6M1, but a lower 28-day compressive strength. The reason could be that while a high alkaline dosage accelerates the reaction process, it also tends to form more porous structures and cause the precipitation of free alkalis, which will ultimately result in slow growth of long-term strength [54].

Finally, the influence of silicate modulus on hydration heat release is demonstrated in Figure **9(g)** and **9(h)**. At the early stage, mix N8M0.75 exhibits the highest and earliest heat release rate peak, while mix N8M1.25 shows a highly delayed and weaker peak. This is because a lower silicate modulus can increase solution alkalinity, accelerating the dissolution of GGBS reactive components and thus intensifying early reaction [55]. The results agree with the UCS results that mix N8M1.25 shows almost negligible UCS after 7-day curing due to the high silicate modulus. The heat release peak occurs after around 350 hours, where the reaction of mixes N8M0.75 and N8M1 stagnates. This could be caused by that a higher silicate modulus provides additional reactive silicate ions, which support late-stage reaction [41]. Finally, mix N8M1.25 accumulates the most hydration heat, followed by mixes N8M1 and N8M0.75. This agrees well with the compressive strength results as well as the setting time results.

3.6. Thermo-Gravimetry Analysis (TGA)

The TGA results were derived by quantifying the characteristic peak area (30 ^{o}C-220 ^{o}C) corresponding to C-(A)-S-H gel, which acts as the primary strength-contributing hydration product in the investigated CLSM system. The C-A-S-H contents in various CLSM are shown in Figure **10**. These TGA results align with the 28-day cumulative hydration heat as well as the 28-day compressive strength. The CLSM with higher cumulative hydration heat exhibits more C-(A)-S-H. Specifically, increasing the binder dosage, replacing soil with coal bottom ash (CBA), elevating the alkaline dosage, and increasing the alkali modulus all enhance C-(A)-S-H formation.

The increase ratio of C-(A)-S-H content in CLSM samples after 12 wet-dry cycles was also investigated, as illustrated in Figure **11**. The results indicate that the amount of C-(A)-S-H increases following 12 wet-dry cycles, which can be attributed to the continuous hydration of unreacted GGBS particles driven by

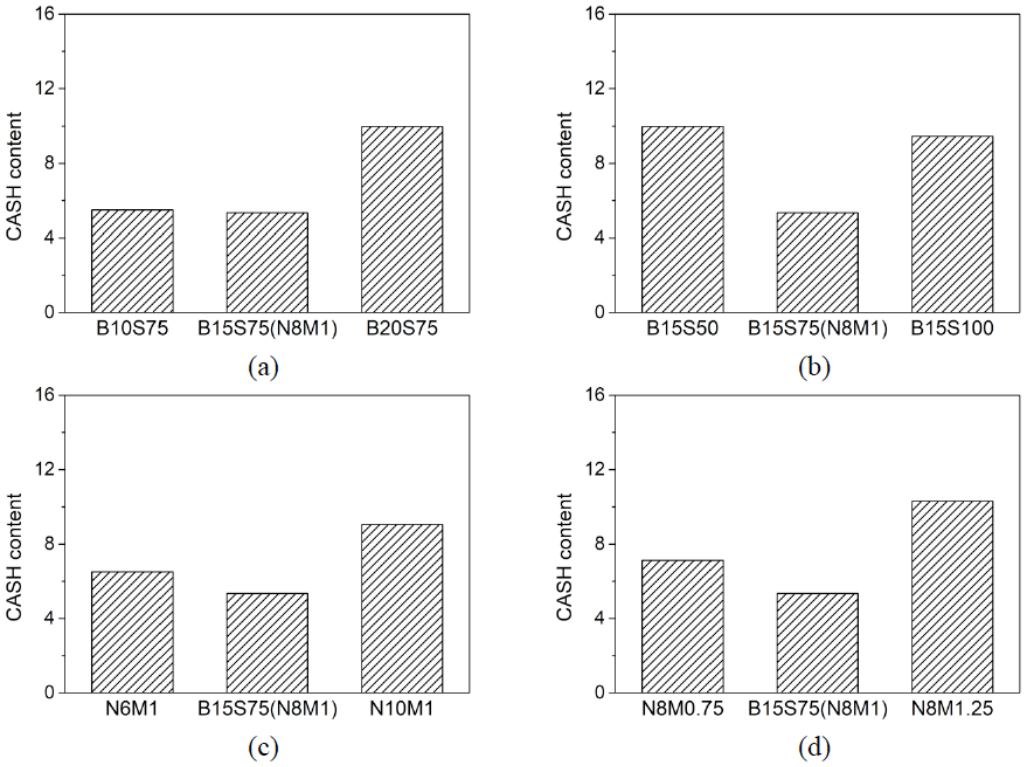

Figure 10: C-(A)-S-H contents in the CLSM at 28 days.

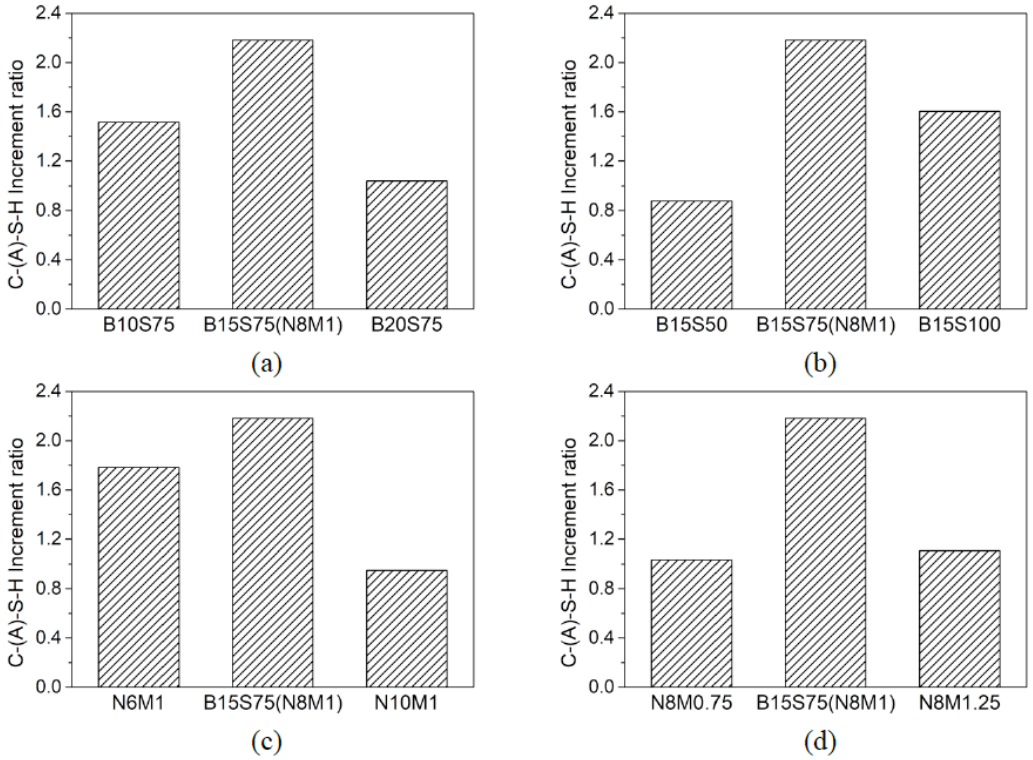

Figure 11: Increase of the C-(A)-S-H ratio in the CLSM at 28 days after wet-dry cycles.

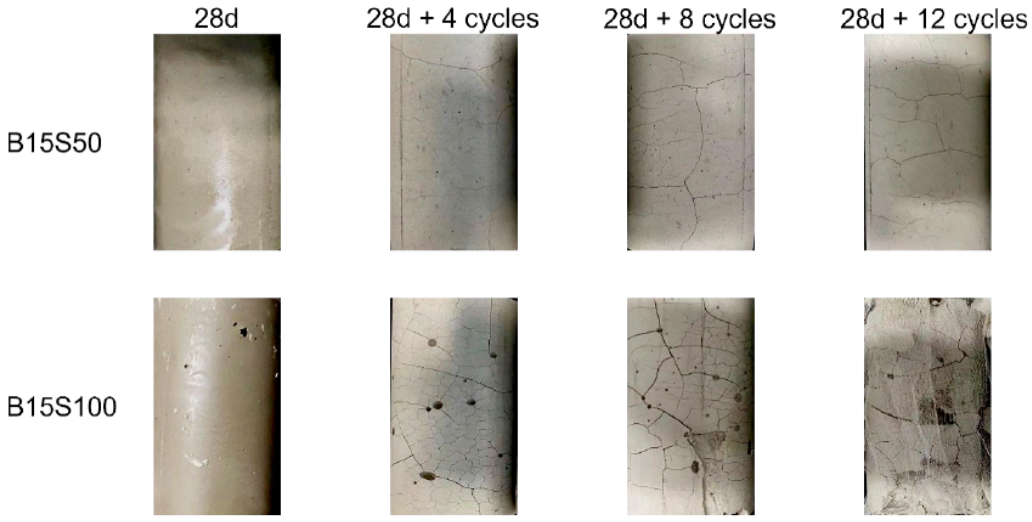

Figure 12: Appearance of CLSM samples before and after wet-dry cycles.

alternating water ingress and thermal activation. The supplementary formation of cementitious products facilitates the enhancement of mechanical properties. For instance, the UCS of mixes B20S75, B15S100, and B15S50 increase after four wet-dry cycles. However, while wet-dry cycles enhance hydration product formation to some extent, it also introduces more defects into the material. The wet-dry cycles lead to repeated cycles of dehydration shrinkage and rehydration expansion within the material. These processes generate cracks that propagate and interconnect under sustained wet-dry exposure (see Figure **12**), ultimately forming a dense crack network and severely compromising the overall mechanical performance. A comparison of the appearance of mixes B15S100 and B15S50 in Figure **12** reveals that mix B15S100 exhibits significantly faster crack propagation and wider crack widths than mix B15S50. Consequently, mix B15S100 shows a more pronounced UCS reduction under wet-dry cycles. This may be ascribed to the finer particle size and stronger hydrophilicity compared to CBA. The cyclic swelling and shrinkage of hydrophilic clay minerals with finer particles would be more easily to induce expansion and matrix potentials [56].

4. CONCLUSIONS

This research proposes and develops a novel alkali-activated CLSM synergising high-viscosity excavated soil, GGBS, and CBA. Experiments were carried out to evaluate the impacts of mix design parameters (*e.g.*, binder content, soil-to-aggregate ratio, alkaline dosage, silicate modulus) and wet-dry cycles on the mechanical properties, while hydration heat and TG analysis could provide further mechanistic insights. This work can provide valuable insights into the composition-property relationships of the novel CLSM and provide practical guidance for its engineering design. The key conclusions are summarised below:

1) CBA exerts the most pronounced effect on the flowability of CLSM. Replacing 50% of the soil with CBA improves the flowability by approximately 77.8%, whereas the influence of GGBS content, alkaline dosage, and silicate modulus is negligible.

2) A greater CBA content leads to an accelerated reaction rate, an increased cumulative heat release, and enhanced formation of C-(A)-S-H gel. These improvements are ultimately reflected in the shortened setting time, enhanced 7-day and 28-day compressive strengths, and improved durability under wet-dry cycles, albeit the effect of CBA content on these properties is relatively limited.

3) A higher GGBS content accelerates hydration, increases cumulative heat release, and thereby enhances the compressive strength of CLSM. However, higher GGBS content makes the CLSM more sensitive to wet-dry cycles, which could be ascribed to the resulting increase in shrinkage under the drying process.

4) A higher alkaline dosage accelerates early hydration, leading to shortened setting time and enhanced 7-day compressive strength. However, higher alkaline dosage may inhibit later-stage reactions, but CLSM with higher alkaline dosage still shows higher 28-day compressive strength. Additionally, the increased alkaline dosage raises the sensitivity of CLSM to wet-dry cycles, which is likely attributable to enhanced shrinkage susceptibility.

5) A lower silicate modulus leads to an earlier and higher heat release peak, contributing to higher 7-day strength of CLSM. In contrast, a higher modulus significantly delays and weakens early reactions, resulting in nearly negligible 7-day compressive strength. However, after approximately 350 hours, the CLSM with a higher silicate modulus begins to release heat, accumulates greater total hydration heat by 28 days, and ultimately achieves higher compressive strength. Therefore, a lower silicate modulus helps reduce setting time and improve early strength, while a higher modulus supports greater later strength.

6) Wet-dry cycles have a dual impact on the long-term strength of CLSM. The wetting phase promotes further hydration, while the drying phase induces and propagates internal microcracks. As the cycles continue, the damaging effect of crack propagation outweighs the strengthening effect of hydration, therefore, resulting in a strength degradation ultimately.

The developed CLSM can be used for backfill applications without mechanical compaction, particularly for trenches, irregular basements, and pipelines. However, it is essential to regulate the mechanical properties of CLSM based on design and excavation requirements. Moreover, the volumetric stability of the CLSM needs to be further investigated, as AAS generally exhibits higher shrinkage than OPC.

ACKNOWLEDGEMENT

Financial support from the Ningbo Municipal Bureau of Science and Technology (Nos.: 2024QL039, 2023Z148, 2024Z258) and the Zhejiang Provincial Department of Science and Technology (Nos.: 2025C02257(SD2) and 2023C03146) is gratefully acknowledged. This paper is also supported by the Ningbo Key Professional Think Tank “Centre for Low Carbon Economy and Scientific Innovation, University of Nottingham Ningbo China”.

REFERENCES

[1] Wang, B., Xiao, J., Zheng, Z., Gan, W., Shen, J., & Wang, J. (2025). Assessment of construction spoil generation: A case study in China. Journal of Cleaner Production, 532, 146879. https://doi.org/10.1016/j.jclepro.2025.146879

[2] Wang, H., Zhang, N., Duan, H., & Dong, L. (2024). Pathways to sound management of excavated soil and rock: A case study in Shenzhen. Journal of Cleaner Production, 458, 142383. https://doi.org/10.1016/j.jclepro.2024.142383

[3] Cristóbal, J., Foster, G., Caro, D., Yunta, F., Manfredi, S., & Tonini, D. (2024). Management of excavated soil and dredging spoil waste from construction and demolition within the EU: Practices, impacts and perspectives. Science of The Total Environment, 944, 173859. https://doi.org/10.1016/j.scitotenv.2024.173859

[4] Zhu, Y., Liu, D., Fang, G., Wang, H., & Cheng, D. (2022). Utilization of excavated loess and gravel soil in controlled low strength material: Laboratory and field tests. Construction and Building Materials, 360, 129604. https://doi.org/10.1016/j.conbuildmat.2022.129604

[5] Luo, W., Liu, S., Hu, Y., Hu, D., Kow, K. W., Pang, C., & Li, B. (2022). Sustainable reuse of excavated soil and recycled concrete aggregate in manufacturing concrete blocks. Construction and Building Materials, 342, 127917. https://doi.org/10.1016/j.conbuildmat.2022.127917

[6] Luo, W., Liu, S., Jiang, Y., Guan, X., Hu, Y., Hu, D., & Li, B. (2021). Utilisation of dewatered extracted soil in concrete blocks produced with Portland cement or alkali-activated slag: Engineering properties and sustainability. Case Studies in Construction Materials, 15, e00760. https://doi.org/10.1016/j.cscm.2021.e00760

[7] Liu, S., Zhang, W., Xu, M., Wang, F., Hu, Y., & Li, B. (2024). Development of cold-bond artificial aggregate with excavated soil and alkali-activated slag. Case Studies in Construction Materials, 21, e03451. https://doi.org/10.1016/j.cscm.2024.e03451

[8] Yan, N., Li, G., Qin, F., Qiao, X., Lu, B., Liang, N., & Zhao, S. (2025). Study on the deformation characteristics of diaphragm walls in deep excavations within the Ningbo soft soil region. Scientific Reports, 15(1), 15036. https://doi.org/10.1038/s41598-025-95878-y

[9] Mahmoud, A., Olivier, J., Vaxelaire, J., & Hoadley, A. F. (2012). Advances in mechanical dewatering of wastewater sludge treatment. In Wastewater reuse and management (pp. 253-303). Dordrecht: Springer Netherlands. https://doi.org/10.1007/978-94-007-4942-9_9

[10] Aziz, M., Sheikh, F. N., Qureshi, M. U., Rasool, A. M., & Irfan, M. (2021). Experimental study on endurance performance of lime and cement-treated cohesive soil. KSCE Journal of Civil Engineering, 25(9), 3306-3318. https://doi.org/10.1007/s12205-021-2154-7

[11] Kim, Y. S., Do, T. M., Kim, H. K., & Kang, G. (2016). Utilization of excavated soil in coal ash-based controlled low strength material (CLSM). Construction and Building Materials, 124, 598-605. https://doi.org/10.1016/j.conbuildmat.2016.07.053

[12] DeLeo, P. C., Baveye, P., & Ghiorse, W. C. (1997). Use of confocal laser scanning microscopy on soil thin-sections for improved characterization of microbial growth in unconsolidated soils and aquifer materials. Journal of Microbiological Methods, 30(3), 193-203. https://doi.org/10.1016/S0167-7012(97)00065-1

[13] Kaliyavaradhan, S. K., Ling, T. C., Guo, M. Z., & Mo, K. H. (2019). Waste resources recycling in controlled low-strength material (CLSM): A critical review on plastic properties. Journal of Environmental Management, 241, 383-396. https://doi.org/10.1016/j.jenvman.2019.03.017

[14] Sheen, Y. N., Zhang, L. H., & Le, D. H. (2013). Engineering properties of soil-based controlled low-strength materials as slag partially substitutes to Portland cement. Construction and Building Materials, 48, 822-829. https://doi.org/10.1016/j.conbuildmat.2013.07.046

[15] He, Z., Zhu, X., Wang, J., Mu, M., & Wang, Y. (2019). Comparison of CO2 emissions from OPC and recycled cement production. Construction and Building Materials, 211, 965-973. https://doi.org/10.1016/j.conbuildmat.2019.03.289

[16] Roy, D. M. (1999). Alkali-activated cements opportunities and challenges. Cement and Concrete Research, 29(2), 249-254. https://doi.org/10.1016/S0008-8846(98)00093-3

[17] Provis, J. L. (2018). Alkali-activated materials. Cement and Concrete Research, 114, 40-48. https://doi.org/10.1016/j.cemconres.2017.02.009

[18] Thomas, R. J., Ye, H., Radlinska, A., & Peethamparan, S. (2016). Alkali-activated slag cement concrete. Concrete International, 38(1), 33-38. https://doi.org/10.14359/51688712

[19] Yang, K. H., Song, J. K., & Song, K. I. (2013). Assessment of CO2 reduction of alkali-activated concrete. Journal of Cleaner Production, 39, 265-272. https://doi.org/10.1016/j.jclepro.2012.08.001

[20] Tan, Y., He, Y., Cui, X., & Liu, L. (2024). The influence of different water glass moduli on the chemical corrosion resistance of alkali-activated porous concrete. Construction and Building Materials, 415, 134971. https://doi.org/10.1016/j.conbuildmat.2024.134971

[21] Lee, N. K., Kim, H. K., Park, I. S., & Lee, H. K. (2013). Alkali-activated, cementless, controlled low-strength materials (CLSM) utilizing industrial by-products. Construction and Building Materials, 49, 738-746. https://doi.org/10.1016/j.conbuildmat.2013.09.002

[22] Fang, S., Lam, E. S. S., Li, B., & Wu, B. (2020). Effect of alkali contents, moduli and curing time on engineering properties of alkali activated slag. Construction and Building Materials, 249, 118799. https://doi.org/10.1016/j.conbuildmat.2020.118799

[23] Lang, L., Chen, B., & Chen, B. (2021). Strength evolutions of varying water content-dredged sludge stabilized with alkali-activated ground granulated blast-furnace slag. Construction and Building Materials, 275, 122111. https://doi.org/10.1016/j.conbuildmat.2020.122111

[24] Wan, X., Ding, J., Jiao, N., Zhang, S., Wang, J., & Guo, C. (2023). Preparing controlled low strength materials (CLSM) using excavated waste soils with polycarboxylate superplasticizer. Environmental Earth Sciences, 82(9), 214. https://doi.org/10.1007/s12665-023-10884-5

[25] Khadka, S. D., Okuyucu, O., Jayawickrama, P. W., & Senadheera, S. (2023). Controlled low strength materials (CLSM) activated with alkaline solution: Flowability, setting time and microstructural characteristics. Case Studies in Construction Materials, 18, e01892. https://doi.org/10.1016/j.cscm.2023.e01892

[26] Shin, Y., Jang, J. G., Choi, J., Jun, G., Park, C., Kim, G. M., & Yang, B. (2023). Utilization of artificial interior stone sludge as fine aggregate in controlled low-strength material (CLSM). Journal of Building Engineering, 71, 106441. https://doi.org/10.1016/j.jobe.2023.106441

[27] Ali, H. A., Zhang, B., Xiao, C., Zhao, B., Xuan, D., & Poon, C. S. (2022). Valorization of fine recycled C&D aggregate and incinerator bottom ash for the preparation of controlled low-strength material (CLSM). Cleaner Waste Systems, 3, 100061. https://doi.org/10.1016/j.clwas.2022.100061

[28] Singh, M. (2018). Coal bottom ash. In Waste and supplementary cementitious materials in concrete (pp. 3-50). Woodhead Publishing. https://doi.org/10.1016/B978-0-08-102156-9.00001-8

[29] Lakhiar, M. T., Bai, Y., Wong, L. S., Paul, S. C., Anggraini, V., & Kong, S. Y. (2022). Mechanical and durability properties of epoxy mortar incorporating coal bottom ash as filler. Construction and Building Materials, 315, 125677. https://doi.org/10.1016/j.conbuildmat.2021.125677

[30] Wu, J. Q., Li, B., Chen, Y. T., & Ghiassi, B. (2023). Investigation on the roles of glass sand in sustainable engineered geopolymer composites. Construction and Building Materials, 363, 129576. https://doi.org/10.1016/j.conbuildmat.2022.129576

[31] Guan, X., Luo, W., Liu, S., Hernandez, A. G., Do, H., & Li, B. (2023). Ultra-high early strength fly ash-based geopolymer paste cured by microwave radiation. Developments in the Built Environment, 14, 100139. https://doi.org/10.1016/j.dibe.2023.100139

[32] ASTM D6103-17; Standard Test Method for Flow Consistency of Controlled Low Strength Material (CLSM). ASTM International: West Conshohocken, PA, USA, 2017.

[33] GB/T 1346-2024: Test methods for water requirement of standard consistency, setting time and soundness of the Portland cement. Standardization Administration and General Administration of Quality Supervision, Inspection and Quar-antine of China, Beijing, China, 2011.

[34] ASTM, D4832. Standard Test Method for Preparation and Testing of Controlled Low Strength Material (CLSM) Test Cylinders. ASTM International: West Conshohocken, PA, USA, 2002.

[35] ASTM D559/D559M-15. Standard Test Methods for Wetting and Drying Compacted Soil-Cement Mixtures. ASTM International: West Conshohocken, PA, USA, 2023.

[36] Rafeet, A., Vinai, R., Soutsos, M., & Sha, W. (2019). Effects of slag substitution on physical and mechanical properties of fly ash-based alkali activated binders (AABs). Cement and Concrete Research, 122, 118-135. https://doi.org/10.1016/j.cemconres.2019.05.003

[37] Lakhiar, M. T., Bai, Y., Wong, L. S., Paul, S. C., Anggraini, V., & Kong, S. Y. (2022). Mechanical and durability properties of epoxy mortar incorporating coal bottom ash as filler. Construction and Building Materials, 315, 125677. https://doi.org/10.1016/j.conbuildmat.2021.125677

[38] Nedunuri, A. S. S. S., & Muhammad, S. (2021). Fundamental understanding of the setting behaviour of the alkali activated binders based on ground granulated blast furnace slag and fly ash. Construction and Building Materials, 291, 123243. https://doi.org/10.1016/j.conbuildmat.2021.123243

[39] Chang, J. J. (2003). A study on the setting characteristics of sodium silicate-activated slag pastes. Cement and Concrete Research, 33(7), 1005-1011. https://doi.org/10.1016/S0008-8846(02)01096-7

[40] Kaze, C. R., Djobo, J. N. Y., Nana, A., Tchakoute, H. K., Kamseu, E., Melo, U. C., ... & Rahier, H. (2018). Effect of silicate modulus on the setting, mechanical strength and microstructure of iron-rich aluminosilicate (laterite) based-geopolymer cured at room temperature. Ceramics International, 44(17), 21442-21450. https://doi.org/10.1016/j.ceramint.2018.08.205

[41] Ouyang, X., Ma, Y., Liu, Z., Liang, J., & Ye, G. (2019). Effect of the sodium silicate modulus and slag content on fresh and hardened properties of alkali-activated fly ash/slag. Minerals, 10(1), 15. https://doi.org/10.3390/min10010015

[42] Qi, W., Duan, G., Han, Y., Zhao, Q., Huang, Y., Zhu, W., ... & Zhang, J. (2024). Comparison of mechanical properties and microstructure of GGBS-based cementitious materials activated by different combined alkaline wastes. Construction and Building Materials, 422, 135784. https://doi.org/10.1016/j.conbuildmat.2024.135784

[43] Huang, Y., Gong, A., Jin, Z., Peng, Y., Shao, S., & Yong, K. (2025). Synergistic Effects of Alkali Activator Dosage on Carbonation Resistance and Microstructural Evolution of Recycled Concrete: Insights from Fractal Analysis and Optimal Threshold Identification. Buildings, 15(10), 1742. https://doi.org/10.3390/buildings15101742

[44] Gebregziabiher, B. S., Thomas, R. J., & Peethamparan, S. (2016). Temperature and activator effect on early-age reaction kinetics of alkali-activated slag binders. Construction and Building Materials, 113, 783-793. https://doi.org/10.1016/j.conbuildmat.2016.03.098

[45] Adewumi, A. A., Mohd Ariffin, M. A., Maslehuddin, M., Yusuf, M. O., Ismail, M., & Al-Sodani, K. A. A. (2021). Influence of silica modulus and curing temperature on the strength of alkali-activated volcanic ash and limestone powder mortar. Materials, 14(18), 5204. https://doi.org/10.3390/ma14185204

[46] Hu, W., Li, K., Yin, W., Zhang, H., Xue, Y., Han, Y., & Liu, P. (2024). Effects of wetting–drying cycles on the macro and micro properties of the cement-stabilized soil with curing agent. Buildings, 14(6), 1716. https://doi.org/10.3390/buildings14061716

[47] He, J., Bai, W., Zheng, W., He, J., & Sang, G. (2021). Influence of hydrated lime on mechanical and shrinkage properties of alkali-activated slag cement. Construction and Building Materials, 289, 123201. https://doi.org/10.1016/j.conbuildmat.2021.123201

[48] Ye, H., & Huang, L. (2020). Shrinkage characteristics of alkali-activated high-volume fly-ash pastes incorporating silica fume. Journal of Materials in Civil Engineering, 32(10), 04020307. https://doi.org/10.1061/(ASCE)MT.1943-5533.0003384

[49] Liu, Y., Feng, S., & Liu, H. (2024). Measurements of drying and wetting gas diffusion coefficients and gas permeability of unsaturated soils using a new flexible-wall device. Journal of Geotechnical and Geoenvironmental Engineering, 150(11), 06024006. https://doi.org/10.1061/JGGEFK.GTENG-12475

[50] Kim, H. K., & Lee, H. K. (2018). Hydration kinetics of high-strength concrete with untreated coal bottom ash for internal curing. Cement and concrete composites, 91, 67-75. https://doi.org/10.1016/j.cemconcomp.2018.04.017

[51] Cai, G. H., Zhou, Y. F., Li, J. S., Han, L. J., & Poon, C. S. (2022). Deep insight into mechanical behavior and microstructure mechanism of quicklime-activated ground granulated blast-furnace slag pastes. Cement and Concrete Composites, 134, 104767. https://doi.org/10.1016/j.cemconcomp.2022.104767

[52] Kim, H. K., & Lee, H. K. (2018). Hydration kinetics of high-strength concrete with untreated coal bottom ash for internal curing. Cement and Concrete Composites, 91, 67-75. https://doi.org/10.1016/j.cemconcomp.2018.04.017

[53] Tiu, E. S. K., Raman, S. N., Kong, D., Sofi, M., & Geng, G. (2025). Correlating the reactivity and strength development of coal bottom ash and coal fly ash in cementitious system. Construction and Building Materials, 466, 140318. https://doi.org/10.1016/j.conbuildmat.2025.140318

[54] Zhang, M., Zunino, F., Yang, L., Wang, F., & Scrivener, K. (2023). Understanding the negative effects of alkalis on long-term strength of Portland cement. Cement and Concrete Research, 174, 107348. https://doi.org/10.1016/j.cemconres.2023.107348

[55] Shi, Z., Shi, C., Wan, S., & Zhang, Z. (2018). Effects of alkali dosage and silicate modulus on alkali-silica reaction in alkali-activated slag mortars. Cement and Concrete Research, 111, 104-115. https://doi.org/10.1016/j.cemconres.2018.06.005

https://doi.org/10.66000/2819-828X.2025.01.08